Semiclassical analysis of Harper-like models

Armelle Barelli and Robert Fleckinger
Laboratoire de Physique Quantique, Université Paul Sabatier, 118 route de Narbonne, F-31062 Toulouse CEDEX, France
(Received 9 April 1992; revised manuscript received 22 July 1992)

The band spectrum of a Bloch electron in a uniform magnetic field is numerically computed for models with third-nearest-neighbor interactions, permitting the effects of geometrical frustration. Unusual contacts between two bands are found and explained by use of semiclassical calculations. Above a given hopping-term magnitude, we observe a braiding of Dirac sublevels.

I. INTRODUCTION

Since the early works of Landau[1] in 1930 and Peierls[2] in 1933, the problem of an electron in a crystal lattice under a uniform magnetic field has been extensively studied. These studies have led to deep insights in the physics of electrons in solids (description of the Fermi surface, de Haas–van Alphen effect, etc.). In 1976, Hofstadter[3] computed the numerical spectrum of the Harper model[4] and discovered its fractal structure. Experimental discoveries such as the quantum Hall effect and high-T_c superconductivity, have stimulated further theoretical works (e.g., flux phases of the Hubbard model[5] and anyon superconductivity[6]).

The Hamiltonian describing the quantum behavior of two-dimensional (2D) Bloch electrons in a uniform magnetic field depends only upon the quasimomentum operator

$$\tilde{K}_\mu = \frac{a}{\hbar}(P_\mu - eA_\mu), \quad \mu = 1,2 ,$$

where A_μ is the vector potential such that $\mathbf{B} = \mathrm{curl}\,\mathbf{A}$, a is the lattice spacing, e is the electric charge, and $\hbar$ is Planck's constant divided by 2π. The quasimomentum components satisfy the commutation rules

$$[\tilde{K}_1, \tilde{K}_2] = \frac{ieBa^2}{\hbar} = 2i\pi\frac{\phi}{\phi_0} = 2i\pi\alpha = i\gamma , \tag{1}$$

where ϕ is the flux per unit cell and $\phi_0 = h/e$ is the flux quantum.

It is important to notice that $\tilde{K}_1$ and $\tilde{K}_2$ appear as conjugate dynamical variables, with the magnetic flux γ playing the role of Planck's constant. For this reason we shall call the semiclassical limit the limit obtained by taking $\gamma \mapsto 0$.

The nesting properties of Hofstadter's spectrum were interpreted by the renormalization-group analysis of Wilkinson.[7] Let us also mention the mathematical work of Helffer and Sjöstrand using pseudo-differential-operator techniques.[8]

For $\gamma = 2\pi p/q$ ($p/q \in \mathbb{Q}$), the Hamiltonian H is periodic so that Bloch's theory applies; therefore H may be written as a $q \times q$ matrix whose entries are periodic functions of $\tilde{K}_\mu$, $\mu = 1,2$.

Another approach has been developed by Rammal and Bellissard,[9] who use an algebraic formalism (for a mathematical overview see Ref. 10) to extend the semiclassical calculations.[11,12] Very recently, this semiclassical analysis has been tested on a triangular lattice[13] and on a square lattice modified by second-nearest-neighbor interactions.[14]

The γ quantum mechanics reveals the topological structure of subbands for $\phi = 0$ or ϕ rational. The nature of points in phase space can be determined by an inspection of the spectrum of the Hamiltonian as a function of the magnetic flux. Extrema of the energy band surfaces in phase space give rise to Landau levels with slope given by the local curvature.

The appearance of saddle points is revealed by a certain thickness of the spectrum; Helffer and Sjöstrand[8] studied these regions of the spectrum, which contribute to the main part of its fractal dimension.[15] When subbands are touching, the generic contact is conical giving rise to Dirac sublevels described by Helffer and Sjöstrand and Rammal and Bellissard for Hofstadter's model.

The tunneling effect between degenerate extrema is revealed by the broadening of Landau levels. This remark is the basis of the renormalization-group analysis of Wilkinson[7] which have been rigorously investigated by Helffer and Sjöstrand.[8] This effect has been illustrated by Barelli and Kreft[14] in a model for which close degenerate minima exist in the unit cell. The study of the action integral between them shows the existence of a real part which produces oscillations of the level splitting when varying the magnetic field.

In the present work we want to complete the previous scheme by introducing a realistic model with third-nearest-neighbor interactions with a hopping term of size t_3. When t_3 is turned on we are faced with nongeneric properties in the spectrum such as various kinds of contact between subbands near rational flux, existence of exact degeneracy of contacts leading to a tunneling effect between Dirac sublevels, and the observation of corresponding spectacular braids.

The flux-phases theory allows one to reduce the study of Hubbard or t-J models to a Harper-like model for which the magnetic flux becomes a dynamical variable minimizing the Fermi-sea energy. In the Harper model with nearest-neighbor interactions, it has been proved numerically[16] and by using the semiclassical approach[9] that the Fermi-sea energy reaches the minimum when the

magnetic flux is equal to the filling factor. This is a basic property for the interpretation of anyon theory.

If we take the third-nearest-neighbor interactions into account, a geometrical frustration effect (when $t_3<0$) may appear, modifying the previous result. This was found by Nori, Douçot, and Rammal[17] in a model Hamiltonian with second- and third-nearest-neighbor interactions. When the Hamiltonian is explicitly flux dependent and for $t_3<0$, we observe a paramagnetic behavior of the electronic gas.

The paper is organized as follows. In Sec. II, we briefly recall the construction of Hamiltonians for two-dimensional electrons subjected to a uniform magnetic field. Section III is devoted to the introduction of our three models with third-nearest-neighbor interactions. We give in Sec. IV some results of the semiclassical calculations. In Sec. V we study the nongeneric band touchings at half-flux. The braiding of Dirac sublevels is explained in Sec. VI. Finally, in Sec. VII, the paramagnetic effect is shown for the model whose Hamiltonian depends upon the magnetic flux γ.

II. ALGEBRAIC SEMICLASSICAL APPROACH

Let us consider the case of a 2D square lattice with spacing a in a magnetic field $\mathbf{B}$. The Hamiltonian operator can be written as

$$H(\mathbf{x},\mathbf{p})=\frac{[\mathbf{p}-q\,\mathbf{A}(\mathbf{x})]^2}{2m^*}+V(\mathbf{x})\ , \tag{2}$$

where $\mathbf{A}(\mathbf{x})$ is the vector potential in any suitable gauge and $V(\mathbf{x})$ is the crystal scalar potential with periodicity a in both dimensions.

Since we are interested only in the tight-binding approximation, the $\mathbf{x}$ position variables take values on the lattice sites indexed by two integers (m,n). When $B=0$, Schrödinger's equation [for any $\psi\in l^2(\mathbb{Z}^2)$] reduces to

$$\begin{aligned}(H\psi)(m,n)=&\,t_1[\psi(m-1,n)+\psi(m+1,n)+\psi(m,n-1)+\psi(m,n+1)]\\&+t_2[\psi(m-2,n)+\psi(m+2,n)+\psi(m,n-2)+\psi(m,n+2)]\\&+t_3[\psi(m-2,n-1)+\psi(m-2,n+1)+\psi(m+2,n-1)\\&+\psi(m+2,n+1)+\psi(m-1,n+2)+\psi(m-1,n-2)+\psi(m+1,n-2)+\psi(m+1,n+2)]\ ,\end{aligned} \tag{3}$$

where t_1,t_2, and t_3 are the hopping strengths of first-, second-, and third-nearest-neighbor interactions.

The Hamiltonian can be expressed as an algebraic combination of the two fundamental translation operators

$$\begin{aligned}(T_1\psi)(m,n)&=\psi(m-1,n)\ ,\\(T_2\psi)(m,n)&=\psi(m,n-1)\ .\end{aligned} \tag{4}$$

By taking into account the periodicity of the lattice, the wave functions are written as Bloch functions:

$$\psi_{k_1,k_2}(m,n)=C_{k_1,k_2}e^{i(k_1m+k_2n)}\ ,$$

where $(k_1,k_2)\in[0,2\pi]\times[0,2\pi]$ are Brillouin-zone variables. This transformation reduces the Hamiltonian to a Bloch Hamiltonian:

$$\begin{aligned}\tilde{\mathfrak{H}}(k_1,k_2)=&\,2t_1(\cos k_1+\cos k_2)+2t_2[\cos(2k_1)+\cos(2k_2)]\\&+2t_3[\cos(2k_1+k_2)+\cos(2k_1-k_2)+\cos(2k_2+k_1)+\cos(2k_2-k_1)]\ .\end{aligned} \tag{5}$$

Since we are dealing with electrons in a uniform magnetic field, we introduce the magnetic translation operators[18]

$$\begin{aligned}(U_1\psi)(m,n)&=\exp\left[\frac{-ie}{\hbar}\int_{(m-1,n)}^{(m,n)}\mathbf{A}\cdot\mathbf{d}l\right]\psi(m-1,n)\ ,\\(U_2\psi)(m,n)&=\exp\left[\frac{-ie}{\hbar}\int_{(m,n-1)}^{(m,n)}\mathbf{A}\cdot\mathbf{d}l\right]\psi(m,n-1)\ ,\end{aligned} \tag{6}$$

where U_1 and U_2 satisfy the following commutation rules:

$$U_1U_2=e^{i\gamma}U_2U_1,\quad \gamma=2\pi\frac{\phi}{\phi_0}=2\pi\phi\frac{e}{h}\ , \tag{7}$$

and $\phi=a^2B$ is the magnetic flux through the unit cell.

This model may be studied by using the method introduced by Rammal and Bellissard[9] which consists of considering U_1 and U_2 as members of an abstract noncommutative C^*-algebra $\mathcal{A}_\gamma$, called the rotation algebra. The main interest of such an algebraic approach is that it allows the generalization of the semiclassical approximation near zero flux to any quasirational magnetic flux so that one can obtain an expansion of the Bloch Hamiltonian matrix in small parameter $\alpha'=|\alpha-p/q|$.

Let us give some details upon the construction of the Bloch Hamiltonian matrix in the general case. It is useful to introduce Weyl's operator

$$W(m_1,m_2)=U_1^{m_1}U_2^{m_2}e^{-i\pi\alpha m_1m_2}\ , \tag{8}$$

satisfying the product rule

$$W(m_1,m_2)W(m_1',m_2') = e^{i\pi\alpha(m_1'm_2-m_2'm_1)}W(m_1+m_1',m_2+m_2') .$$

Then, given a classical Hamiltonian $\mathfrak{H}$, we get, for its Fourier transform,

$$(\mathfrak{H})(k_1,k_2)=\sum_{(m_1,m_2)\in\mathbb{Z}^2} a(m_1,m_2)e^{i(k_1m_1+k_2m_2)} ,$$

and associate this expansion with the following matrix Hamiltonian:

$$H=\sum_{(m_1,m_2)\in\mathbb{Z}^2} a(m_1,m_2)e^{i(k_1m_1+k_2m_2)}w_1^{m_1}w_2^{m_2} \times e^{-i\pi\alpha m_1m_2} , \quad (9)$$

with

$$w_1=\begin{bmatrix} 0 & 1 & 0 & \cdots & 0 \\ 0 & 0 & 1 & & 0 \\ 0 & 0 & 0 & & 0 \\ \vdots & & & \ddots & \vdots \\ 0 & & & & 1 \\ 1 & 0 & 0 & \cdots & 0 \end{bmatrix} \in M_{q\times q} ,$$

$$w_2=\begin{bmatrix} 1 & & & & \\ & e^{2i\pi p/q} & & & \\ & & \ddots & & \\ & & & e^{2i\pi(p/q)(q-1)} & \end{bmatrix} \in M_{q\times q} . \quad (10)$$

In our example, we get

$$H(k_1,k_2)=t_1(e^{ik_1}w_1+e^{ik_2}w_2)+t_2(e^{2ik_1}w_1^2+e^{2ik_2}w_2^2) +t_3(e^{2ik_1}e^{ik_2}w_1^2w_2e^{-i\gamma}+e^{2ik_1}e^{-ik_2}w_1^2w_2^{-1}e^{i\gamma}+e^{2ik_2}e^{ik_1}w_2^2w_1e^{-i\gamma}+e^{2ik_2}e^{-ik_1}w_2^2w_1^{-1}e^{i\gamma})+\text{H.c.} \quad (11)$$

The spectrum of H is computed using algorithms for matrix diagonalization. We have performed diagonalizations up to $q=40$ for the entire spectrum. We have performed matrix diagonalizations up to $q=100$ near half-flux when we wanted to zoom near points of interest. This approach has been tested on different models.[5,9,13,14]

The semiclassical calculation, namely, the expansion modulo $O(\gamma^\infty)$, can be done by using Peierls' substitution (rigorously justified in Refs. 9 and 10):

$$k_i \mapsto k_{ic}+\sqrt{\gamma}K_i \quad \text{with } i=1,2 , \quad (12)$$

where k_{ic}, $i=1,2$, are bottom well coordinates in phase space and K_i are operators obeying Heisenberg's commutation rules, namely

$$[K_1,K_2]=i . \quad (13)$$

The expansion near $\gamma=0$ leads to an effective Hamiltonian. Then, we obtain the energies modulo $O(\gamma^\infty)$ using perturbation theory.

Near a rational flux $\gamma=2\pi p/q+\gamma'$ the previous substitution is replaced by

$$k_i \mapsto k_{ic}+\sqrt{\gamma'}K_i \quad \text{with } i=1,2 . \quad (14)$$

The effective Hamiltonian obtained after the expansion is then an operator-valued $q\times q$ matrix. Using Schur's-complement method, we reduce the Hamiltonian to one band edge and diagonalize it to obtain the corresponding energies.

III. GEOMETRICAL DESCRIPTION OF THE MODELS

To introduce the different models we want to deal with, let us recall the second- and third-nearest-neighbor tight-binding Hamiltonian in a uniform magnetic field B, through the magnetic translation operators U_j, $j=1,2$, defined by Eq. (6) and setting $t_1=1$:

$$H=U_1+U_2+t_2(U_1^2+U_2^2) +t_3(U_1^2U_2+U_1^2U_2^{-1}+U_2^2U_1+U_2^2U_1^{-1})+\text{H.c.} \quad (15)$$

When $t_2=t_3=0$, we recover the well-known Hofstadter's model[3] with its corresponding spectrum looking like a butterfly; for $t_3=0$ and $t_2\neq0$ Barelli and Kreft[14] computed the spectrum and exhibited the braiding structure of the Landau sublevels due to tunneling effects in phase space for particular values of t_2; the case $t_2,t_3\neq0$ has been studied by Nori, Douçot, and Rammal.[17] They pointed out that effect of the geometrical frustration

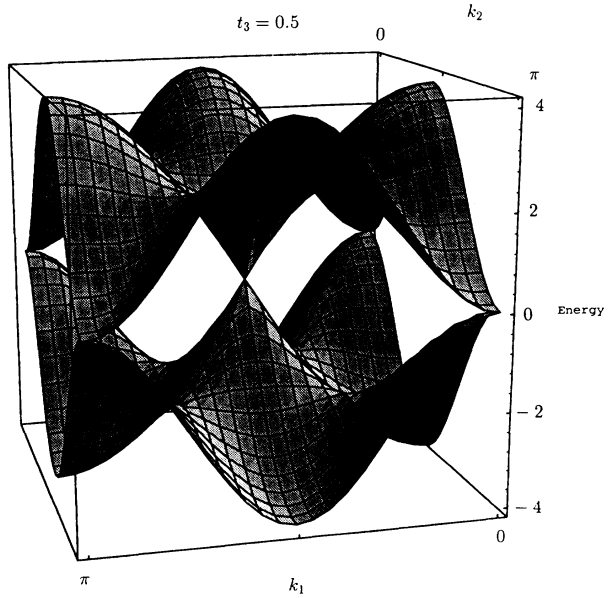

FIG. 1. Parabolic contacts between energy subbands at half-flux for the knight's-move model when $t_3=\frac{1}{2}$.

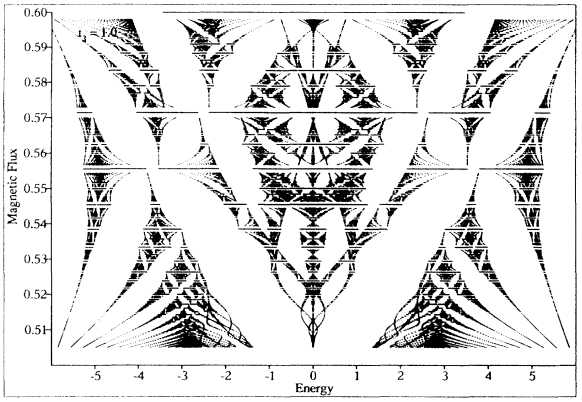

FIG. 2. Braiding of Dirac sublevels emerging from zero energy at half-flux for the knight's-move model when $t_3=1$.

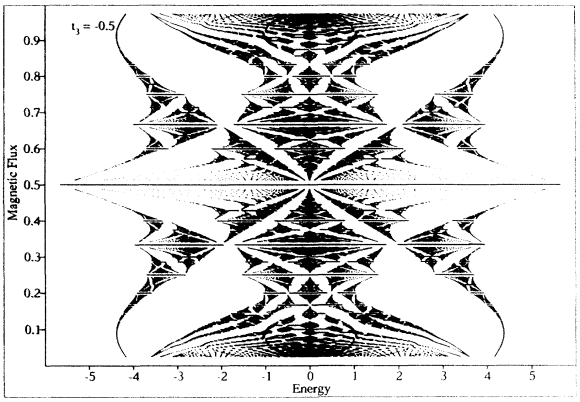

FIG. 3. Paramagnetism phenomenon in the γ-dependent model for $t_3=-\frac{1}{2}$. We have checked that the susceptibility is negative at low fields.

$(t_2>0,\ t_3<0)$ on the ground-state energy.

Here we consider the case $t_2=0$, $t_3\neq 0$ (either positive or negative). The third-nearest-neighbor interaction permits it to exhibit nongeneric behavior like parabolic contacts near half-flux (Fig. 1) and the braiding structure of Dirac sublevels (Fig. 2). In this class of models it is possible to introduce a geometrical frustration by setting $t_3<0$. This produces a paramagnetic behavior of the electronic gas (Fig. 3).

To illustrate this class of models let us introduce what we will call the "knight's-move model" by analogy with the knight's move (KM) on a chessboard. Using the rules previously mentioned the classical Hamiltonian is expressed as

$$\mathfrak{H}_{\mathrm{KM}}(k_1,k_2)=2\cos k_1+2\cos k_2 +2t_3[\cos(2k_1+k_2)+\cos(2k_1-k_2) +\cos(2k_2+k_1)+\cos(2k_2-k_1)]\ . \tag{16}$$

And we will consider a model for which the classical Hamiltonian explicitly depends upon the magnetic flux $\gamma=2\pi\alpha$:

$$\mathfrak{H}_{\mathrm{KM},\gamma}(k_1,k_2,\gamma)=2\cos k_1+2\cos k_2+2t_3[\cos(k_1+2k_2-2\gamma) +\cos(k_1-2k_2+2\gamma)+\cos(2k_1+k_2-2\gamma)+\cos(2k_1-k_2+2\gamma)]\ . \tag{17}$$

In the weak-magnetic-field limit we recover the knight's-move model described by Eq. (16).

IV. LEVELS NEAR ZERO AND HALF-FLUXES; TUNNELING EFFECT

In this section we review for our model the properties already investigated in previous works: Landau levels near $\alpha=0$ and $\frac{1}{2}$, and Landau "braids" near $\alpha=0$.

A. Topology of bands near zero flux

The location and nature of critical points for $\mathfrak{H}_{\mathrm{KM}}(k_1,k_2)$ are summarized in Table I. As in the model studied in Ref. 14 there is a bifurcation for a special value of t_3. For example, we observe that for $t_3=-\frac{1}{10}$ four degenerate minima $(\pi,\pm\alpha_2),(\pm\alpha_2,\pi)$ with α_2 appear such that $\cos\alpha_2=(1+2t_3)/8t_3$. The consequence of such a bifurcation on the structure of the spectrum has been explained in Ref. 14. For $t_3<-\frac{1}{10}$, the corresponding spectrum is shown in Fig. 4 and exhibits braidlike structure for given values of the energy.

B. Landau sublevels near zero flux

By computing $\mathfrak{H}_{\mathrm{KM}}$ near the critical points (minima or maxima), quantizing and expanding near $\gamma=0$ up to order 1 (see Appendix A) we obtain the energies

(k_{1c},k_{2c})	$E_n^{\mathrm{KM}}(\gamma)$
(0,0)	$4+8t_3-\gamma(1+10t_3)(2n+1)$
(π,π)	$-4-8t_3+\gamma(1+10t_3)(2n+1)$
$(\pi,\pm\alpha_2),(\pm\alpha_2,\pi)$	$\frac{36t_3^2-12t_3+1}{8t_3}-\frac{3\gamma}{32t_3}(6t_3-1)(10t_3+1)(2n+1)$
$(0,\pm\alpha_1),(\pm\alpha_1,0)$	$-\frac{36t_3^2-12t_3+1}{8t_3}+\frac{3\gamma}{32t_3}(6t_3-1)(10t_3+1)(2n+1)$

(18)

TABLE I. Location and nature of the critical points of the knight's-move model Hamiltonian near zero flux. Here $\alpha_1=\arccos[(-1-2t_3)/8t_3]$, $\alpha_2=\arccos[(1+2t_3)/8t_3]$, $\alpha_3=\arccos(2t_3-1)/12t_3$, $\alpha_4=\arccos[-(2t_3-1)/12t_3]$.

Critical points \ t_3	$-\infty$	$-\frac{1}{10}$	0	$\frac{1}{6}$	$\frac{1}{2}$	$+\infty$
(0,0)	min	max	max	max	max	
$(0,\pi),(\pi,0)$	Saddle point					
(π,π)	max			min		
$(0,\pm\alpha_1),(\pm\alpha_1,0)$	max	Undefined			min	
$(\pi,\pm\alpha_2),(\pm\alpha_2,\pi)$	min	Undefined			max	
$(\pm\alpha_3,\pm\alpha_3),(\pm\alpha_4,\pm\alpha_4)$	Saddle point		Undefined		Saddle point	

To treat the γ-dependent model (17), we had to include an extra term in the semiclassical expansion.[9]

In first order in γ, the Landau levels are given by

$$E_n^{\mathrm{KM},\gamma}(\gamma)=\mathfrak{H}_{\mathrm{KM},\gamma}(k_{1c},k_{2c},0)+C|\gamma|(2n+1)+\gamma\frac{\partial\mathfrak{H}_{\mathrm{KM},\gamma}(k_{1c},k_{2c},0)}{\partial\gamma}+\cdots, \quad (19)$$

where the constant C is explicitly related to the determinant of the Hessian matrix of the quantized version of $\mathfrak{H}_{\mathrm{KM},\gamma}$. In our case it is easy to compute the derivative with respect to the magnetic flux, namely,

$$\frac{\mathfrak{H}_{\mathrm{KM},\gamma}(k_1,k_2,0)}{\partial\gamma}=8t_3\sin k_2(2\cos^2 k_1+2\cos k_2\cos k_1-1)\,. \quad (20)$$

C. "Landau" braids near zero flux

Since the four local extrema (minima or maxima) in the knight's-move model are degenerate, we expect a tunneling effect below $t_3=-\frac{1}{10}$. This tunneling effect leads to a braiding of the four Landau sublevels at small flux. The numerical spectrum obtained by diagonalization of $q\times q$ matrices exhibits the expected behavior near the local minima corresponding to the energy (see Fig. 5 for $t_3=-\frac{1}{2}$)

$$E_0=\frac{36t_3^2-12t_3+1}{8t_3}\,.$$

As studied in Ref. 14, the braid structure can be explained by semiclassical calculations related to tunneling effect in phase space.

Due to the rotational symmetry of our problem, the effective tunneling Hamiltonian denoted by H_T takes the form

$$H_T=\begin{bmatrix}0 & t & r & \bar{t}\\ \bar{t} & 0 & t & r\\ r & \bar{t} & 0 & t\\ t & r & \bar{t} & 0\end{bmatrix}.$$

Here $t=\tau e^{i\theta}$ describes the reduced interaction between two neighboring extrema while $r\in\mathbb{R}$ describes the interaction between second neighbors.

The eigenvalues of the tunneling matrix H_T are

$$\lambda_1=r+2\tau\cos\theta,\quad \lambda_2=r-2\tau\cos\theta\,,$$

$$\lambda_3=-r+2\tau\sin\theta,\quad \lambda_4=-r-2\tau\sin\theta\,.$$

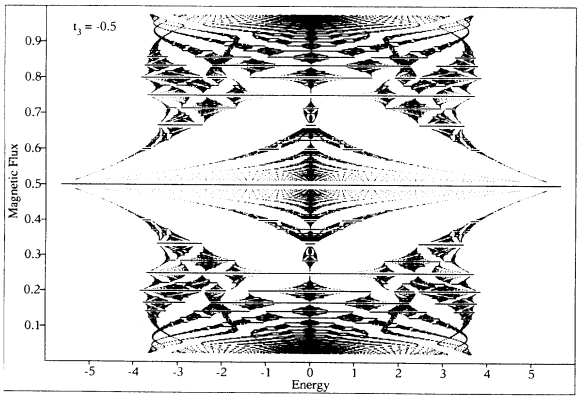

FIG. 4. Spectrum of knight's-move model for $t_3=-\frac{1}{2}$.

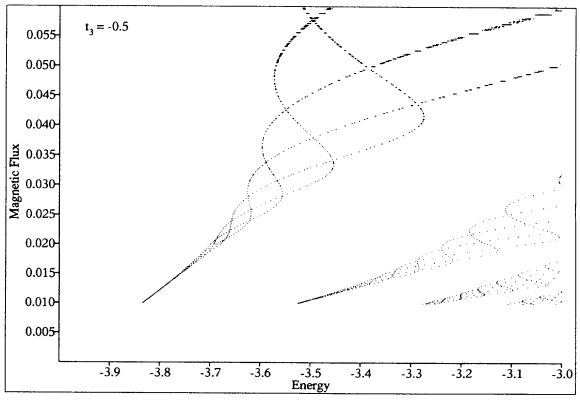

FIG. 5. Braiding of Landau sublevels near zero flux in the knight's-move model for $t_3=-\frac{1}{2}$.

Following the strategy developed by Wilkinson and Austin in Ref. 19 we numerically compute the classical action S along a closed path joining the contours (see Appendix B) and insert it in the expression of the tunneling matrix element τ, namely,

$$\tau=\gamma\frac{\omega}{2\pi}e^{-\mathrm{Im}(S)/\gamma}\ , \tag{21}$$

where ω is the corresponding harmonic-oscillator frequency and the phase θ is defined by

$$4\theta=\frac{\mathrm{Re}(S)}{\gamma}+\pi\ .$$

The eigenvalues of the tunneling matrix H_T give the splitting of energy.

Adding the semiclassical energy obtained in (18) and the contribution due to tunneling effect, we fit to first order in γ the data extracted from the exact spectrum (Fig. 6), by

$$\begin{aligned}\mathfrak{E}_n^{1,2}(\gamma)=&\frac{36t_3^2-12t_3+1}{8t_3}\\&-\frac{3\gamma}{32t_3}(6t_3-1)(10t_3+1)(2n+1)\\&+r\pm\gamma\frac{\omega}{\pi}e^{-\mathrm{Im}(S)/\gamma}\cos\left[\frac{\mathrm{Re}(S)}{4\gamma}+\frac{\pi}{4}\right],\\\mathfrak{E}_n^{3,4}(\gamma)=&\frac{36t_3^2-12t_3+1}{8t_3}\\&-\frac{3\gamma}{32t_3}(6t_3-1)(10t_3+1)(2n+1)\\&+r\pm\gamma\frac{\omega}{\pi}e^{-\mathrm{Im}(S)/\gamma}\sin\left[\frac{\mathrm{Re}(S)}{4\gamma}+\frac{\pi}{4}\right].\end{aligned} \tag{22}$$

The broadening of levels observed in the braids is controlled by $e^{-|\mathrm{Im}(S)|/\gamma}$ while the oscillations are due to the real part of the action $\mathrm{Re}(S)/\gamma$. We numerically checked that the coefficient r is negligible compared with t.

D. Landau sublevels near half-flux

Following the strategy developed in Sec. II near the $\alpha=\frac{1}{2}$ value of the magnetic flux, the Hamiltonian is represented here by a 2×2 matrix and the magnetic

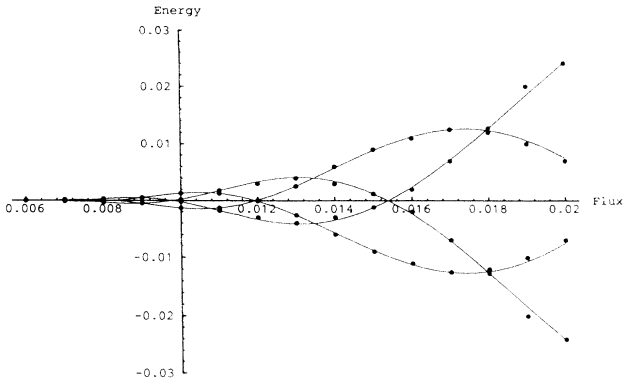

FIG. 6. Comparison between semiclassical calculations (solid curves) and datas extracted from the numerical spectrum (points) for the knight's-move model near zero flux for $t_3=-\frac{1}{2}$.

translation operators are transformed into

$$U_j(k)=e^{ik_j}w_j\quad(k\in\mathbb{T}^2),\quad j=1,2\ ,$$

with

$$w_1=\begin{bmatrix}0&1\\1&0\end{bmatrix}=\sigma_1,\quad w_2=\begin{bmatrix}0&-i\\i&0\end{bmatrix}=\sigma_2\ . \tag{23}$$

σ_1, σ_2, and σ_3 are the usual 2×2 Pauli matrices, with

$$\sigma_3=\begin{bmatrix}1&0\\0&-1\end{bmatrix}\ .$$

Therefore, the Hamiltonian may be rewritten as

$$\begin{aligned}\mathfrak{H}_{\mathrm{KM}}^{\alpha=1/2}(k_1,k_2)=&2[\cos k_1-2t_3\cos k_1\cos(2k_2)]\sigma_1\\&+2[\cos k_2-2t_3\cos(2k_1)\cos k_2]\sigma_2\ .\end{aligned} \tag{24}$$

As in the weak-magnetic-field limit, we compute the eigenvalues of $\mathfrak{H}_{\mathrm{KM}}^{\alpha=1/2}$ to get

$$\begin{aligned}E_{\pm}^{\mathrm{KM}}(k_1,k_2)=&\pm2\{\cos^2k_1[1-2t_3\cos(2k_2)]^2\\&+\cos^2k_2[1-2t_3\cos(2k_1)]^2\}^{1/2}\ .\end{aligned} \tag{25}$$

We also computed the location and nature of critical points for E_+ and E_- when t_3 is varied. The results are summarized in Table II.

For the lowest order in the magnetic flux $\gamma'=\gamma-\pi$, the semiclassical calculations give

(k_{1c},k_{2c})	$E_n^{\mathrm{KM}}(\gamma')$
$(\pm\pi/2,\pm\pi/2)$	$2\sqrt{2}(1+2t_3)\sqrt{\gamma' n}$
(β_2,β_2)	$2\sqrt{2}(1+2t_3)\sqrt{(2t_3-1)/t_3}\sqrt{\gamma' n}$
$(0,0),(0,\pi),(\pi,0),(\pi,\pi)$	$2\sqrt{2}\lvert1-2t_3\rvert+O(\gamma')$
$(0,\pi/2),(\pi/2,0),(\pi,\pi/2),(\pi/2,\pi)$	$2\lvert1+2t_3\rvert+O(\gamma')$

(26)

We find the emergence of the usual Landau levels and of two families of Dirac points giving rise to a $\sqrt{\gamma'}$ behavior.[9,8]

TABLE II. Location and nature of the critical points of the knight's-move model Hamiltonian near half-flux. Here $\beta_1=\arccos[(12t_3^2+12t_3-1)/32t_3^2]$, $\beta_2=\arccos[\pm(1+2t_3)/4t_3]$, and $\beta_3=\arccos[\pm(1+2t_3)/12t_3]$.

Critical points \ t_3	$-\infty$	$-\frac{3+2\sqrt{3}}{6}$	$-\frac{1}{2}$	0	$\frac{2\sqrt{3}-3}{6}$	$\frac{1}{10}$	$\frac{1}{2}$	$+\infty$
$(0,0),(0,\pi),(\pi,0),(\pi,\pi)$	max	max	max	max	max	min		max
$(0,\pi/2),(\pi/2,0),(\pi,\pi/2),(\pi/2,\pi)$	max	Saddle point				max		
$(\pm\pi/2,\pm\pi/2)$				min				
$(\pi/0,\pm\beta_1),(\pm\beta_1,\pi/0)$	Saddle			Undefined				Saddle point
(β_2,β_2)		min		Undefined				min
(β_3,β_3)		Saddle point		Undefined				Saddle point

V. NONGENERIC CONTACTS AT HALF-FLUX

In this section we study the band touching in the particular case $\alpha=\gamma/2\pi=\frac{1}{2}$. We find parabolic contacts (Fig. 1) giving rise to Landau levels in the corresponding spectrum (Fig. 7).

A. Contact along lines

The computation of the critical points of $E_{\pm}^{\mathrm{KM}}(k_1,k_2)$ requires us to treat as a particular case the band touching for $t_3=-\frac{1}{2}$. Then the eigenvalues of the classical Hamiltonian (24) computed at $\alpha=\frac{1}{2}$ are

$$E_{\pm}^{\mathrm{KM}}(k_1,k_2)=\pm 2\sqrt{\cos^2 k_1[1+\cos(2k_2)]^2+\cos^2 k_2[1+\cos(2k_1)]^2}\ . \tag{27}$$

We notice that the band touching arises along two lines of critical points determined by $(k_1,\pi/2)$ and $(\pi/2,k_2)$ with (k_1,k_2) in the Brillouin zone, as it is shown by Fig. 8. The associated spectrum is represented in Fig. 4.

B. Parabolic contacts

The semiclassical calculations revealed the emergence of Landau levels near $\alpha=\frac{1}{2}$ (26). For $t_3=\frac{1}{2}$, these levels correspond to zero energy and the observation of subbands contacts suggests a new kind of behavior. In this case Eq. (25) becomes

$$E_{\pm}^{\mathrm{KM}}(k_1,k_2)=\pm 2\{\cos^2 k_1[1-\cos(2k_2)]^2+\cos^2 k_2[1-\cos(2k_1)]^2\}^{1/2}\ . \tag{28}$$

Near the points

$$(0,0),\ (\pi,0),\ (0,\pi),\ \text{and}\ (\pi,\pi)\ ,$$

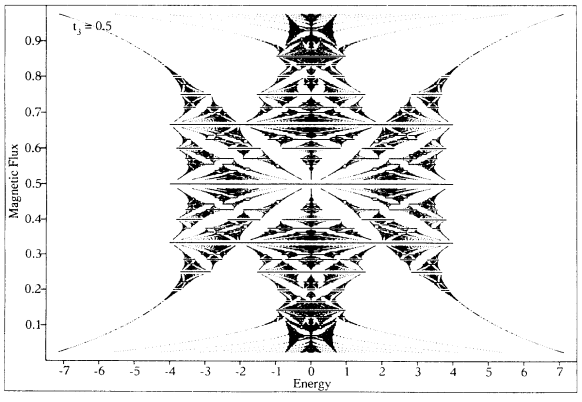

FIG. 7. Spectrum of knight's-move model for $t_3=\frac{1}{2}$.

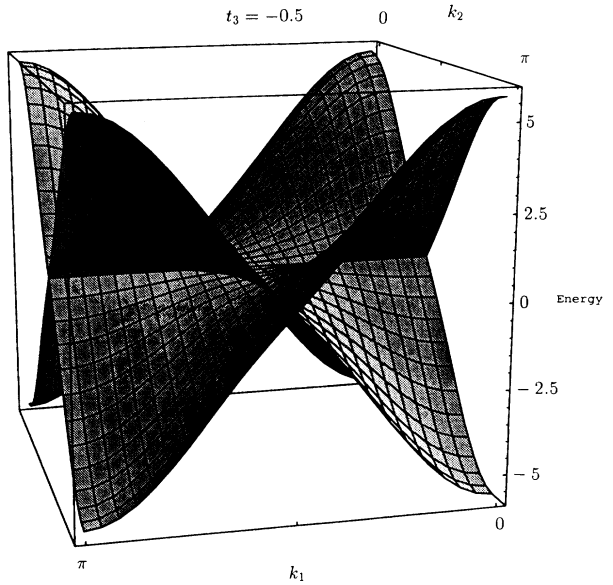

FIG. 8. Subbands contact along two perpendicular lines in the knight's-move model at half-flux for $t_3=-\frac{1}{2}$.

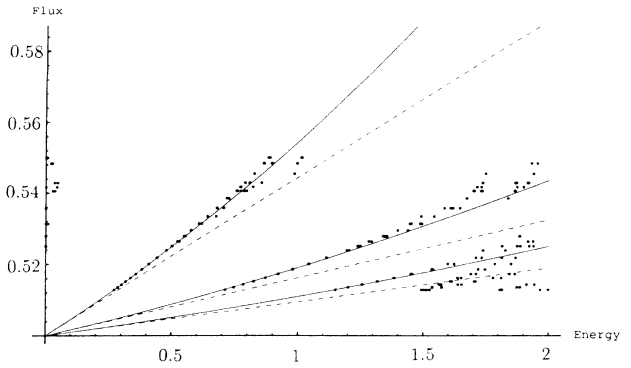

FIG. 9. Comparison between semiclassical calculations (dashed lines) and datas extracted from the exact spectrum (points) for the parabolic subband contacts near half-flux in the knight's-move model for $t_3=\frac{1}{2}$. Solid lines correspond to the addition of a fitted γ^2 term in the semiclassical expansion.

we observe a parabolic contact (Fig. 1) and the quantized Hamiltonian can be rewritten in the lowest order in γ' as

$$H_{\mathrm{KM}}^{\left[\begin{smallmatrix}\pi & \pi\\ 0 & 0\end{smallmatrix}\right]}(\gamma')=4\gamma'(K_2^2\sigma_1+K_1^2\sigma_2)=4\gamma' H_0 \ . \tag{29}$$

The eigenvalues of $H_0^2=K_1^4+K_2^4+2(K_1K_2+K_2K_1)$ were numerically computed; the lowest corresponding eigenvalues are 0.800 807 8, 6.041 937, and 17.673 803. From these results we perform a numerical comparison between the exact spectrum and the semiclassical results (Fig. 9). Dots represent the exact spectrum, dashed lines the semiclassical expansion up to order one in γ, and solid curves contain a correction of order γ^2.

The nature of the contact can be easily determined by an expansion given by the following rule: let η be the small parameter such that $k_{1c,2c}$ is replaced by $k_{1c,2c}^{\mathrm{contact}}+\eta$. Performing the calculation in the limit $\eta\mapsto 0$ we find the following expressions (up to order 4 in η):

$$E_+^{\mathrm{KM}}(\eta,\eta)=2\sqrt{2}\left|2\eta^2-\tfrac{5}{3}\eta^4\right| \ . \tag{30}$$

The η^2 behavior for E_+ explains the parabolic contact between the two subbands.

VI. TUNNELING BETWEEN DIRAC LEVELS

The aim of this section is to explain the braiding structure observed in Fig. 2. As has been done in Sec. IV C, we compute an effective tunneling Hamiltonian (4×4 matrix) and apply Wilkinson and Austin's result to get the tunneling matrix element.

A. Conical contacts

Let us consider the case $t_3\neq\pm\frac{1}{2}$ in the knight's-move model near half-flux. The equation for band touching, $E_+(k_1,k_2)=E_-(k_1,k_2)$, has the following solutions:

$$(k_{1c},k_{2c})=(\pm\pi/2,\pm\pi/2) \quad \text{for any } t_3$$

and

$$(k_{1c},k_{2c})=(\beta_2,\beta_2) \quad \text{if } t_3\in(-\infty,-\tfrac{1}{2})\cup(\tfrac{1}{2},+\infty) \ .$$

The nature of the contact can be easily determined by expanding around the solutions written above. As was done to exhibit parabolic contacts, we introduce the parameter η and replace $k_{1c,2c}$ by $k_{1c,2c}^{\mathrm{contact}}+\eta$.

When $\eta\mapsto 0$ we find the following expressions up to order 3 in η:

$$\begin{aligned} E_+^{(\pm\pi/2,\pm\pi/2)}(\eta)&=2\sqrt{2}\left|-(1+2t_3)\eta+\frac{26t_3+1}{6}\eta^3\right| \ , \\ E_+^{(\beta_2,\beta_2)}(\eta)&=2\sqrt{2}\left|2\sqrt{(2t_3+1)/4t_3}\,\eta+4\sqrt{(2t_3+1)/4t_3}(1-t_3)\eta^2-\sqrt{(2t_3-1)/4t_3}\,\frac{6t_3^2+17t_3+4}{3t_3}\eta^3\right| \ . \end{aligned} \tag{31}$$

Therefore, the contact is conical at each point where bands touch, as can be seen in Fig. 10 ($t_3=-1$).

B. Braid structure at half-flux

The degeneracy of Dirac points (β_2,β_2) observed for $t_3\geq\frac{1}{2}$ leads to a braiding of the Dirac sublevels emerging from the zero energy (Fig. 2). Such a phenomenon due to the tunneling effect for a rational value of the magnetic flux α has not been seen before. Having a look at Table II, we remark that two bifurcations occur for $t_3=-\frac{1}{2}$ and for $t_3=\frac{1}{2}$ giving rise to four degenerate minima in the Brillouin zone.

As in the zero-field limit, we are able to compute the action along a closed path relating the four degenerate minima (see Appendix B). The main problem here is to adapt formulas computed for a bottom well problem[19] to a Dirac point leading to a $\sqrt{\gamma'}$ behavior [Eq. (26)] for the semiclassical energy.

We compared semiclassical results obtained by diagonalization of the tunneling matrix with the data extracted from the exact spectrum (Fig. 11) using the numerical results for the tunneling action (see Appendix B). To obtain agreement we had to adjust the parameter ω corresponding to the harmonic-oscillator frequency. We notice that for $\alpha>0.515$ the accuracy is lower because the coupling between the four minima and the other minimum $(\pi/2,\pi/2)$ becomes relevant.

VII. PARAMAGNETISM

This section is devoted to the study of the γ-dependent model described by Eq. (17). The corresponding spec-

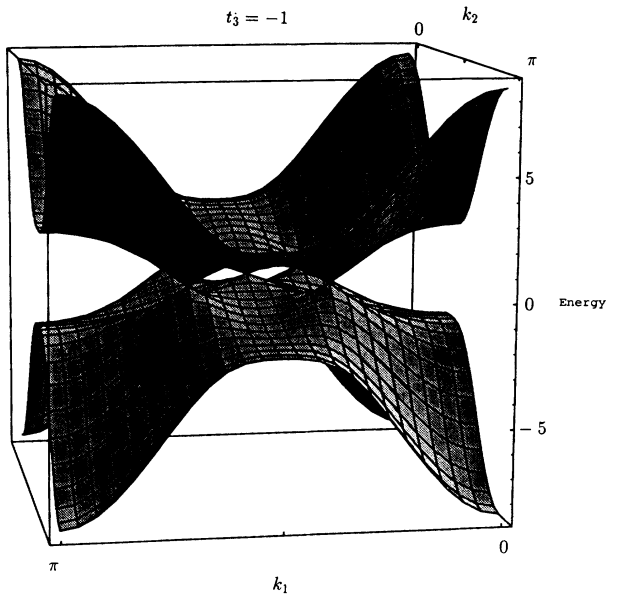

FIG. 10. Conical subbands contacts for the knight's-move model near half-flux for $t_3 = -1$.

trum (see Fig. 3) exhibits paramagnetism as the Fermi-sea energy decreases when increasing the magnetic flux (at low fluxes).

A. Suppression of the tunneling effect

As we said before, the γ-dependent model is reduced to the knight's-move model when $\gamma = 0$. The spectrum has been computed in Fig. 3. The main observation is that there are no braids in spite of the degeneracy of four minima at $\gamma = 0$; this means in particular that there is no tunneling effect in this model in the weak-field limit.

Let us consider, for example, the case of the four minima, namely,

$$(\pi, \pm\alpha_2), (\pm\alpha_2, \pi) \quad \text{such that } \alpha_2 = \arccos\left[\frac{1+2t_3}{8t_3}\right].$$

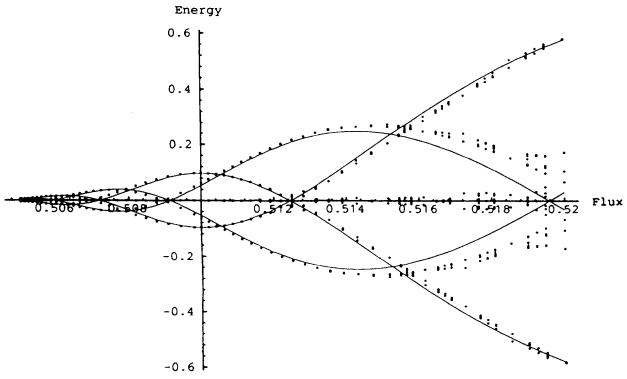

FIG. 11. Comparison between semiclassical calculations (solid lines) and exact spectrum (points) for the braiding Dirac sublevels exhibited by the knight's-move model near half-flux for $t_3 = 1$.

The contributions of each of them to the extra term coming from the γ dependence in Eq. (19) are as follows:

(k_{1c}, k_{2c})	$\frac{\partial \tilde{\Phi}_{\mathrm{KM},\gamma}}{\partial \gamma}$
$(\pi, \pm\alpha_2)$	$\pm(2t_3-1)\sqrt{(10t_3+1)(6t_3-1)/16t_3^2}$
$(\pm\alpha_2, \pi)$	0

(32)

When $t_3 = -\frac{1}{2}$, we can perform an interesting comparison between the spectra of both models in Figs. 4 and 3, respectively. The semiclassical formulas in this case give the following extra terms:

(k_{1c}, k_{2c})	$\frac{\partial \tilde{\Phi}_{\mathrm{KM},\gamma}}{\partial \gamma}$
$(\pi, \pi/2)$	4
$(\pi, 3\pi/2)$	-4
$(\pi/2, \pi), (3\pi/2, \pi)$	0

(33)

Inserting (33) in (19), we obtain to first order in γ' the Landau levels for the minima

(k_{1c}, k_{2c})	$E_n^{\mathrm{KM},\gamma}(\gamma)$
$(\pi, 3\pi/2)$	$-4+\gamma(6n-1)$
$(\pi/2, \pi), (3\pi/2, \pi)$	$-4+3\gamma(2n+1)$
$(\pi, \pi/2)$	$-4+\gamma(6n+7)$

(34)

These expressions fit perfectly with the spectrum. Therefore, we are able to explain the vanishing of the braids because the fourfold degeneracy is partially lifted. The level emerging from -4 on the left side of the spectrum can be explained by the previous formulas. It corresponds to $E_0(\pi, 3\pi/2)$ having a negative slope compared with the other Landau levels. Figure 12 shows the degeneracy of two Landau levels as computed in (34).

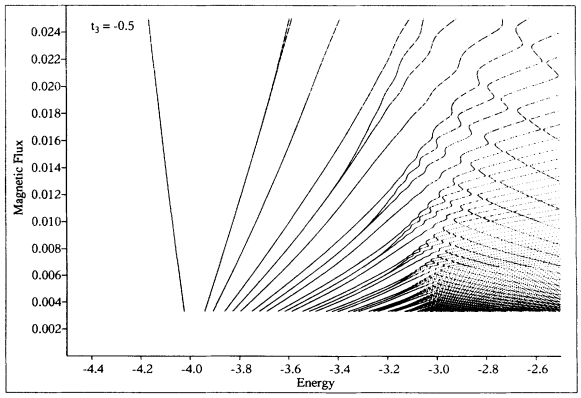

FIG. 12. Vanishing of braids in the γ-dependent model for $t_3 = -\frac{1}{2}$.

B. Landau paramagnetism

The explicit γ dependence of the classical Hamiltonian (17) is found to lead to interesting phenomenon. Models previously investigated (up to second-nearest-neighbor interaction without any explicit dependence in the flux) exhibited "Landau diamagnetism" for the related electronic gas, namely, the Fermi-sea energy (in the weak-magnetic-field limit) $\mathcal{E}(\phi)$ is a function of the magnetic field and

$$\chi=-\frac{\mu_0}{B}\frac{\partial\mathcal{E}}{\partial B}<0 ,$$

where χ is the magnetic susceptibility.

For our γ-dependent model we have a positive value of the magnetization at low fields and hence paramagnetism.

VII. CONCLUSION

This paper presents a detailed study of some characteristic features of the spectra of Bloch electrons in a magnetic field. We focused our work on the effects of a third-nearest-neighbor interaction on the numerical spectrum. We have studied the effects of parabolic contacts between two bands and exhibited a braiding structure of Dirac sublevels due to the tunneling effect near half-flux. We pointed out the accuracy of the semiclassical calculations.

The algebraic techniques permitted us to get an efficient way of computing semiclassical expansions near the bottom of wells and Dirac points. Nevertheless, there is a need for improving these algebraic methods to quantize near a saddle point or a line of critical points.

The semiclassical limit in these models, $\gamma\mapsto 0$, has been studied both with the algebraic approach[9] and in the pseudo-differential-operator framework.[8,20] As far as the WKB method is concerned, let us mention the exhaustive work of Helffer and Sjöstrand for the Harper model.[8]

Finally we exhibited a paramagnetism in the sense that the Fermi-sea energy decreases when the magnetic flux increases. This property, however, needs to be studied more precisely for this type of model.[21]

ACKNOWLEDGEMENTS

We want to thank J. Bellissard for constant support and helpful discussions.

APPENDIX A: QUANTIZATION AND HARMONIC-OSCILLATOR FORMALISM

Near the critical points (k_{1c},k_{2c}) the quantization of $\mathcal{H}$ results from the substitution

$$k_{1,2}\mapsto k_{1c,2c}+\sqrt{\gamma}K_{1,2} ,$$

where K_μ, $\mu=1,2$, are the quasimomentum operator components satisfying the following commutation rules:

$$[K_1,K_2]=i .$$

The semiclassical expansion ($\gamma\mapsto 0$) requires the calculation of matrix elements of the usual harmonic oscillator. Defining creation and annihilation operators we use the standard formalism:

$$K_1=\frac{a+a^*}{\sqrt{2}},\quad K_2=\frac{a-a^*}{i\sqrt{2}}\quad\text{with } [a,a^*]=1 .$$

Let us recall the following rules: $a|n\rangle=\sqrt{n}\,|n-1\rangle$, $a^*|n\rangle=\sqrt{n+1}|n+1\rangle$. Following the strategy developed in Ref. 9, we find

$$\langle n|(K_1^2,+K_2^2)|n\rangle=2n+1 ,$$

$$\langle n|(K_1^4+K_2^4)|n\rangle=\tfrac{3}{4}[1+(2n+1)^2] ,$$

$$\langle n|(K_1^2K_2^2+K_2^2K_1^2)|n\rangle=\tfrac{1}{4}[-3+(2n+1)^2] ,$$

$$\langle n|(K_1K_2^2K_1+K_2K_1^2K_2)|n\rangle=\tfrac{1}{4}[5+(2n+1)^2] ,$$

$$\langle n|(K_1K_2K_1K_2+K_2K_1K_2K_1)|n\rangle=\tfrac{1}{4}[1+(2n+1)^2] .$$

APPENDIX B: COMPUTATION OF COMPLEX PATHS

In this discussion we calculate complex paths and associated action integrals corresponding to situations involving the tunneling effect for zero and half-flux. Concerning the zero flux case the degeneracy in phase space is reached for $t_3\le-\frac{1}{10}$ and $t_3\ge\frac{1}{6}$. To find the path relating the four degenerate wells we have to solve

$$2\cos k_1+2\cos k_2 +4t_3[\cos(2k_1)\cos k_2+\cos(2k_2)\cos k_1]=E_0 , \quad \text{(B1)}$$

where $E_0=(36t_3^2-12t_3+1)/8t_3$. If k_1 is a real number, the previous equation allows k_2 to be complex such that

$$\cos k_2=\frac{-1+2t_3-4t_3\cos^2k_1\pm f(k_1)}{8t_3\cos k_1} , \quad \text{(B2)}$$

where

$$f^2(k_1)=16t_3^2\cos^4k_1-8t_3(1-2t_3)\cos^2k_1 +8t_3E_0\cos k_1+(1-2t_3)^2 .$$

From Table II, we expect braiding of sublevels for $t_3\le-\frac{1}{2}$ and $t_3\ge\frac{1}{2}$. At first order in γ', the equation giving the path relating the four degenerate minima in phase space is

$$\cos^2k_1[1-2t_3\cos(2k_2)]^2 +\cos^2k_2[1-2t_3\cos(2k_1)]^2=0 . \quad \text{(B3)}$$

If k_1 remains real then k_2 may be complex, satisfying

$$\cos^2k_2=\frac{-(1+2t_3)^2-16t_3\cos^2k_1(t_3\cos^2k_1-1-2t_3)\pm g(k_1)}{32t_3^2\cos^2k_1} , \quad \text{(B4)}$$

where

$$g^2(k_1)=[(1+2t_3)^2+16t_3\cos^2k_1(t_3\cos^2k_1-1-2t_3)]^2-64t_3^2(1+2t_3)^2\cos^4k_1 \ .$$

The resulting complex actions satisfy

$$S=\int_{k_{1,\min}}^{k_{1,\max}} k_2(k_1)dk_1 \ . \tag{B5}$$

In the following table, we give the numerical results obtained for the four cases of interest:

	Real part	Imaginary part	Observation
$\alpha=0,\ t_3=-\frac{1}{2}$	2.125 89	−0.141 448	Braids for $q=40$
$\alpha=0,\ t_3=\frac{1}{2}$	1.167 44	−0.331 342	No braids observed
$\alpha=\frac{1}{2},\ t_3=1$	2.707 24	−0.163 531	Braids for $q=100$
$\alpha=\frac{1}{2},\ t_3=-1$	1.370 80	−0.186 932	No braids observed

[1]L. D. Landau, Z. Phys. **64**, 629 (1930).
[2]R. E. Peierls, Z. Phys. **80**, 763 (1933).
[3]D. Hofstadter, Phys. Rev. B **14**, 2239 (1976).
[4]P. G. Harper, Proc. R. Soc. London **68**, 874 (1955).
[5]R. Rammal and J. Bellissard, Europhys. Lett. **13**, 205 (1990).
[6]G. S. Canright, S. M. Girvin, and A. Brass, Phys. Rev. Lett. **63**, 2291 (1983); **63**, 2295 (1983).
[7]M. Wilkinson, Proc. R. Soc. London Ser. A **391**, 305 (1984).
[8]B. Helffer and J. Sjöstrand, Bull. Société Mathématique de France, Tome 116, Fasc. 4, Mémoire 34 (1988); Bull. Société Mathématique de France, Tome 118, Fasc. 1, Mémoire 40 (1990); Bull. Société Mathématique de France, Tome 117, Fasc. 4, Mémoire 43 (1989).
[9]R. Rammal and J. Bellissard, J. Phys. (Paris) **51**, 1803 (1990).
[10]J. Bellissard, in *Operator Algebras and Application,* edited by D. E. Evans and M. Takesaki (Cambridge University Press, Cambridge, 1988), Vol. II.
[11]R. Rammal and J. Bellissard, J. Phys. (Paris) **51**, 2153 (1990).
[12]A. Barelli, J. Bellissard, and R. Rammal, J. Phys. (Paris) **51**, 2167 (1990).
[13]J. Bellissard, C. Kreft, and R. Seiler, J. Phys. A **24**, 2329 (1991).
[14]A. Barelli and C. Kreft, J. Phys. I France **1**, 1229 (1991).
[15]C. Tang and M. Kohmoto, Phys. Rev. B **34**, 2041 (1986).
[16]D. Poilblanc, M. Héritier, G. Montambaux, and P. Lederer, J. Phys. C **19**, L321 (1986).
[17]F. Nori, B. Douçot, and R. Rammal, Phys. Rev. B **44**, 7637 (1991).
[18]J. Zak, Phys. Rev. **134**, A1602 (1964); **134**, A1607 (1964).
[19]M. Wilkinson and E. J. Austin, J. Phys. A **23**, 2529 (1990).
[20]Ph. Briet, J.-M. Combes, and P. Duclos, Comments Partial Differential Equations **12**, 201 (1987).
[21]A. Barelli and R. Fleckinger (unpublished).

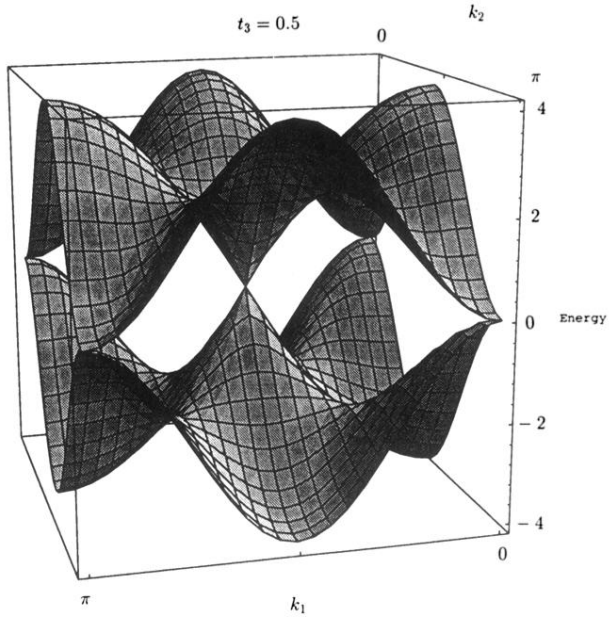

FIG. 1. Parabolic contacts between energy subbands at half-flux for the knight's-move model when $t_3 = \frac{1}{2}$.

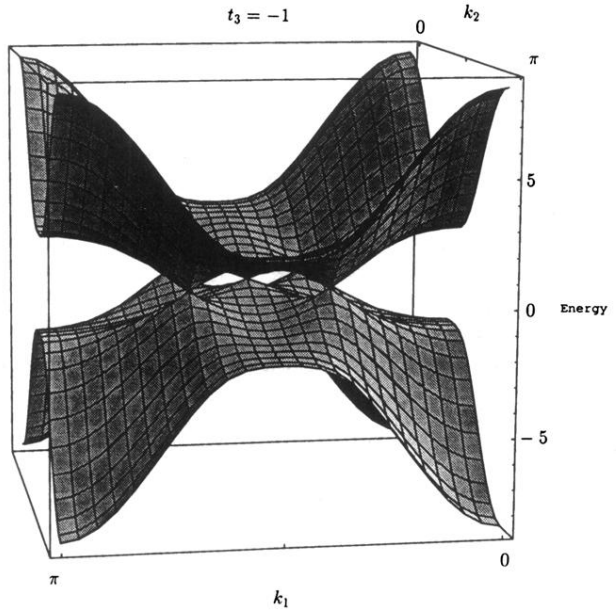

FIG. 10. Conical subbands contacts for the knight's-move model near half-flux for $t_3 = -1$.

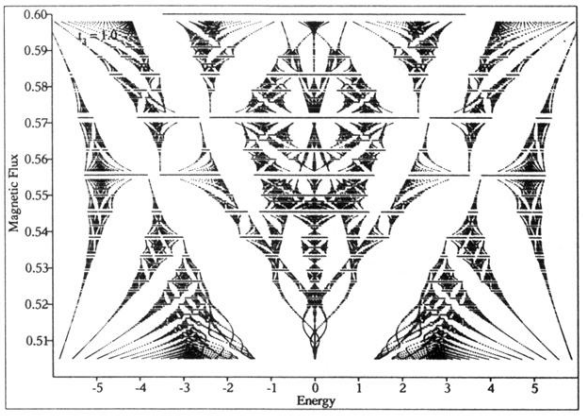

FIG. 2. Braiding of Dirac sublevels emerging from zero energy at half-flux for the knight's-move model when $t_3 = 1$.

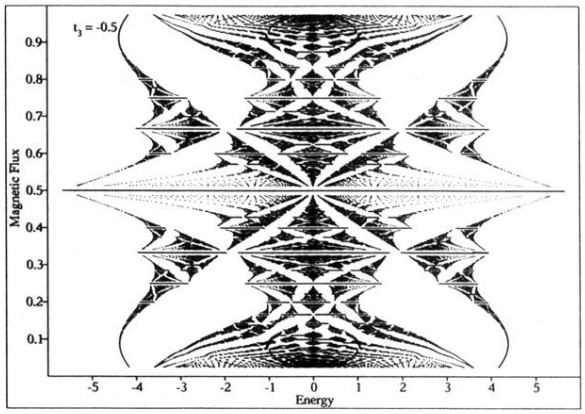

FIG. 3. Paramagnetism phenomenon in the γ-dependent model for $t_3 = -\frac{1}{2}$. We have checked that the susceptibility is negative at low fields.

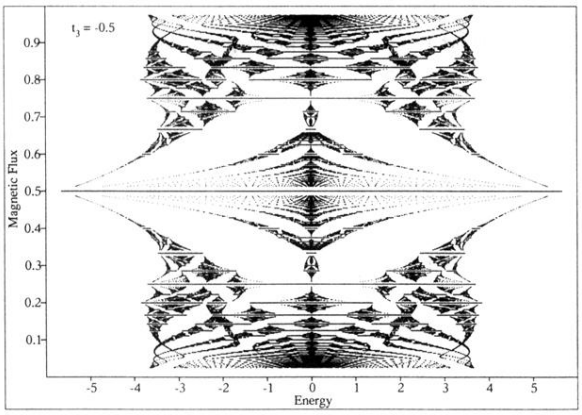

FIG. 4. Spectrum of knight's-move model for $t_3 = -\frac{1}{2}$.

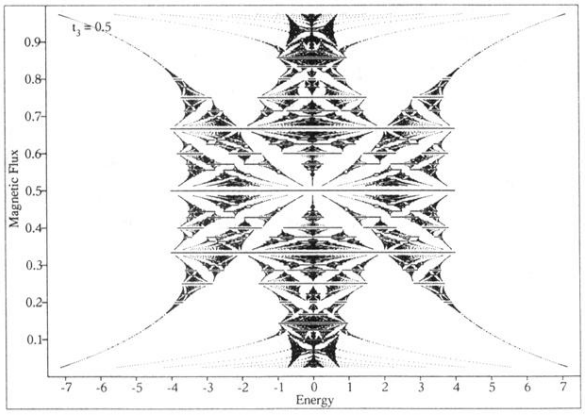

FIG. 7. Spectrum of knight's-move model for $t_3 = \frac{1}{2}$.

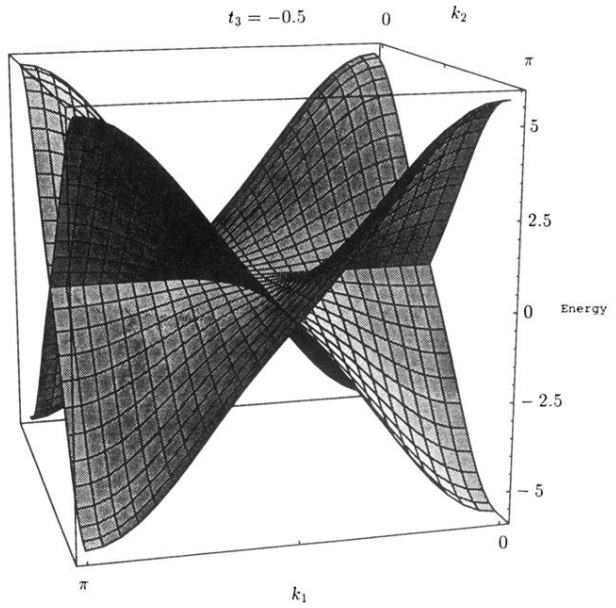

FIG. 8. Subbands contact along two perpendicular lines in the knight's-move model at half-flux for $t_3 = -\frac{1}{2}$.